Journal of Applied Polymer Science

Dielectric properties of graphene–iron oxide/polyimide films with oriented graphene

Ling Ding, Leipeng Liu, Penggang Li, Fengzhu Lv, Wangshu Tong, Yihe Zhang
Beijing Key Laboratory of Materials Utilization of Nonmetallic Minerals and Solid Wastes, National Laboratory of Mineral Materials, School of Materials Science and Technology, China University of Geosciences, Beijing 100083, People's Republic of China
Correspondence to: F. Lv (E-mail: lfz619@cugb.edu.cn) and Y. Zhang (E-mail: zyh@cugb.edu.cn)

ABSTRACT: The preparation of high-dielectric-constant (k) materials is important in the field of electronics. However, how to effectively use the function of fillers to enhance k is still a challenge. In this study, anisotropic graphene (GNS)–iron oxide (Fe_3O_4)/polyimide (PI) nanocomposite films with oriented GNSs were prepared by the *in situ* polymerization of 4,4′-oxydianiline and pyromellitic anhydride in the presence of GNS–Fe_3O_4. Films of the precursors were fabricated, and this was followed by stepwise imidization under a magnetic field at a higher temperature to orient the magnetic sheets. The orientation of GNS–Fe_3O_4 and the relationships of the GNS–Fe_3O_4 content and measurement frequency with the dielectric properties of the GNS–Fe_3O_4/PI films were studied in detail. The dielectric property differences of the GNS–Fe_3O_4/PIs with GNS–Fe_3O_4 parallel or perpendicular to the film surface were not obvious, when the content of GNS–Fe_3O_4 was lower than 5 wt %. However, at the percolation threshold, the k values of GNS–Fe_3O_4/PI films with horizontal GNS–Fe_3O_4 were much higher than those of the other two kinds of films at 10^3 Hz; this was derived from the contribution of more effective microcapcitors parallel to the film surface. So, making the GNS–Fe_3O_4 parallel to the film surface greatly enhanced k of GNS–Fe_3O_4. However, switching the charges on the large lateral surface of the parallel GNSs with the electric field also caused a higher dielectric loss and the frequency dependence of k and the dielectric loss at low frequency. © 2015 Wiley Periodicals, Inc. J. Appl. Polym. Sci. **2016**, *133*, 43041.

KEYWORDS: composites; dielectric properties; films; polyimides

Received 12 June 2015; accepted 28 September 2015
DOI: 10.1002/app.43041

INTRODUCTION

High-dielectric-constant (k) materials are widely used in microelectronics, including bypass capacitors,[1] organic field-effect transistors,[2] organic thin-film electroluminescent devices,[3] electrical stress control applications,[4] actuators,[5] and energy-storage devices.[6–8] As one kind of high-k materials, high-k polymer composites have received increasing interest recently for their high k and easy processing.[9] The introduction of conductive particles into polymer matrix has been proven to be an effective way to form high-k composites; this overcomes the shortcomings, such as the higher filler content, lower mechanical properties, and poor flexibility, of ceramic/polymer composites.[10,11] Until now, many kinds of conductive particles, including Ni,[12] Ag,[13] carbon nanotubes,[14,15] carbon black,[16] exfoliated graphite nanoplates,[10,17,18] and graphene (GNS),[19–22] have been introduced into polymers. Generally, on the basis of percolation theory, the high k in conductor/polymer composites originates from the formation of a percolation network.

The unique structure of exfoliated graphite, which has a large aspect ratio, unique layered structure, and nanoscale thickness, confers advantages for the formation of a large number of parallel microcapacitors[10] and is good for k enhancement.[10,23,24] For example, He *et al.*[10] prepared high-k exfoliated graphite/PVDF (polyvinylidene fluoride) nanocomposites by a solution-casting and hot-pressing technique. The graphite nanoplates were stocked as a sandwich to form a larger number of microcapacitors. Tong *et al.*[25] used spin-assistant preparation and multiple hot pressings to prepare GNS/PVDF–HFP (hexafluoropropylene) composites. The GNS nanosheets were well dispersed and oriented in the films. The unique structure of GNS/PVDF–HFP endowed the composites with a high k. Tian *et al.*[26] introduced thermally expanded GNS nanoplates into poly(dimethyl siloxane) to improve the k. The mechanism of the largely improved dielectric properties in the aforementioned systems was carefully discussed and was considered to be derived from the formation of many parallel microcapacitor structures. However, the kind of microcapacitor good for k improvement has not yet been well understood, or the kind of orientation that the sheets adopt that is beneficial of the improvement of k has not been discussed in detail.

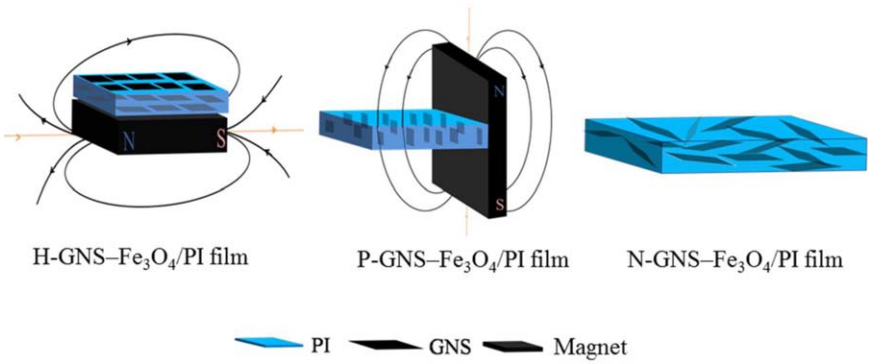

Figure 1. Scheme of the oriented films. [Color figure can be viewed in the online issue, which is available at wileyonlinelibrary.com.]

In this study, GNS–iron oxide (Fe_3O_4)/polyimide (PI) nanocomposites films with GNS orientated parallel or horizontal to the film surface were prepared under the help of a magnetic field in the process of imidization. The effects of the orientation of GNS–Fe_3O_4 in the films, the GNS–Fe_3O_4 content, and the measurement frequency on the dielectric properties were studied. The results indicate that microcapacitors with GNS–Fe_3O_4 parallel to the film surface greatly enhanced k of the composite film because of the large lateral surface of GNS for interfacial polarization. Making lamellar fillers parallel to the film surface greatly enhanced the function of the fillers and endowed the materials with high k values.

EXPERIMENTAL

Materials

Natural flake graphite (300 mesh) was provided by Shuangxing Graphite Processing Plant (China). Iron(III) acetyl acetonate [$Fe(acac)_3$] was obtained from Aldrich. 4,4′-Oxydianiline (ODA) and pyromellitic anhydride (PMDA) were purchased from Mitsubishi Gas Chemical Co., Inc. (Japan). Triethylene glycol and *N,N*-dimethylacetamide (DMAc) were provided by Sinopharm Chemical Reagent Co., Ltd. (China), and DMAc was dried by molecular sieves before use. H_2SO_4 (98%), $KMnO_4$, and H_2O_2 (30%) were obtained from Beijing Chemical Reagent.

Preparation of GNS–Fe_3O_4

The GNS–Fe_3O_4 was synthesized by a hydrothermal method on the basis of the work of He *et al.*,[27] in which the graphene oxide (GO) used was prepared by a modified Hummers method from natural flake graphite.[28] H_2SO_4 (50 mL) was added to a 250-mL flask filled with graphite (2 g) at room temperature; this was followed by the slow addition of solid $KMnO_4$ (7 g) at 0°C. Then, the system was stirred at 35°C for 2 h. Excess water was added to the mixture at 0°C (in an ice bath), and then, H_2O_2 (30 wt % in water) was added until there was no gas produced. After filtration, a brown powder (GO) was produced, and this GO was dried *in vacuo* at room temperature for 12 h. To prepare GNS–Fe_3O_4, the weight ratio of $Fe(acac)_3$ to GO was 2:1. Briefly, 0.1 g of GO and 0.2 g of $Fe(acac)_3$ were added to 75 mL of triethylene glycol and then ultrasonicated for 30 min; this was followed by hydrothermal treatment at 200°C for 12 h in a Teflon-lined stainless steel autoclave (100 mL). The as-prepared powders were collected and washed with deionized water and ethanol repeatedly three times and then vacuum-dried at 60°C to yield GNS–Fe_3O_4.

Preparation of the Anisotropic GNS–Fe_3O_4/PI Composite Films

The anisotropic GNS–Fe_3O_4/PI nanocomposite films with oriented GNSs were prepared by the *in situ* polymerization of ODA and PMDA in the presence of GNS–Fe_3O_4. The fabrication of the films was followed by stepwise imidization under a magnetic field at a higher temperature to orient the GNS–Fe_3O_4 sheets.[29] In a typical operation, 0.1054 g of GNS–Fe_3O_4 was dispersed in 25 mL of treated DMAc and ultrasonicated for 30 min in a three-necked flask (100 mL) at room temperature. Then, 1.0520 g of ODA was dissolved in the previous suspension in the aid of mechanical stirring. An amount of 1.6700 g of PMDA was added slowly within 1 h in an ice bath. The suspension was stirred vigorously at 0°C for 5 h to yield a viscous GNS–Fe_3O_4/poly(amic acid) mixture, which was cast on a clean glass slide to form a uniform film. This was subsequently placed in an oven at 60°C for 30 min to evaporate the partial solvent. Then, the film was oriented horizontal or perpendicular to the glass slide surface with an approximately 0.6-T magnetic field and then imidized at 80, 100, 150, 250, and 300°C for 1 h, respectively, under the magnetic field to form anisotropic GNS–Fe_3O_4/PI films with a thickness of about 50 μm. As shown in Figure 1, the target films oriented with horizontal and perpendicular magnetic fields were designated as H-GNS–Fe_3O_4/PIs and P-GNS–Fe_3O_4/PIs, respectively, and the films without magnetic field treatment were designated as N-GNS–Fe_3O_4/PIs.

Characterization

X-ray diffraction (XRD) patterns were obtained at a scanning rate of 8°/min with a Rigaku D/Max-r A rotating anode X-ray diffractometer with a Cu Kα tube ($\lambda = 1.5405$ Å)and a Ni filter. The average crystallite size of Fe_3O_4 (T) after the assumption of a spherical shape was calculated from the diffraction line width of the XRD patterns on the basis of Scherrer's relation:

$$T = 0.9\mathrm{l}/\beta \cos \theta \quad (1)$$

where θ and β are the diffraction angle and the full width at half maximum, respectively.[30]

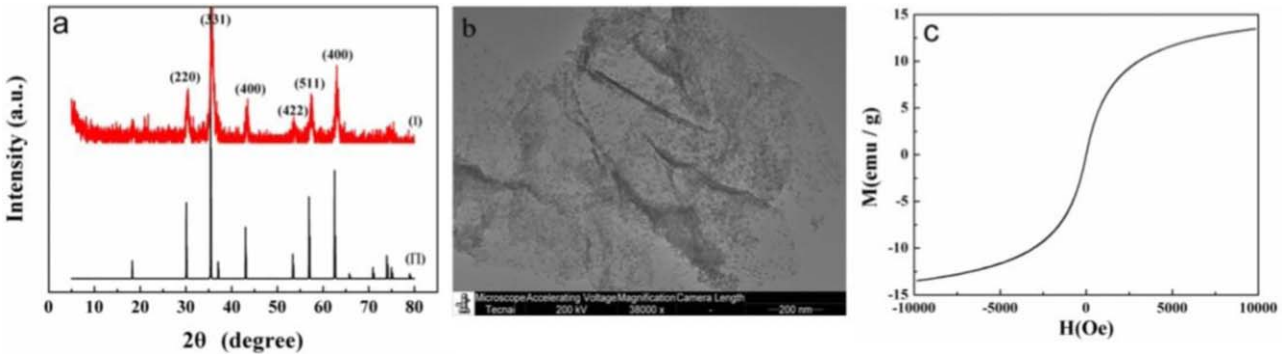

Figure 2. (a) XRD pattern, (b) TEM image, and (c) saturation magnetization of the GNS–Fe_3O_4 hybrid. [Color figure can be viewed in the online issue, which is available at wileyonlinelibrary.com.]

Magnetic hysteresis loops were obtained by a PPMS-9T vibrating sample magnetometer at room temperature. Transmission electron microscopy (TEM; H-8100) was used to observe the morphology of GNS–Fe_3O_4. The fracture surface morphology of the GNS–Fe_3O_4/PI films was observed by a scanning electron microscope (Hitachi S-450, Japan). The dielectric studies were carried out with an impedance gain-phase analyzer (Agilent 4294A) as a function of the frequency (1000 Hz–5 MHz) at room temperature. The relative dielectric constant (ε_r) was estimated with the following equation:

$$\varepsilon_r = \frac{dC_p}{A\varepsilon_0} \tag{2}$$

where C_p is the measured capacitance; d and A are the thicknesses of the composites and the surface of the circular electrodes, respectively; and ε_0 is the dielectric constant of the vacuum (8.854×10^{-12} F/m). The dielectric data in this study was the average of three measurements.

The conductivity (σ) of GNS–Fe_3O_4 was tested with a Corners probe tester (RST-5). The GNS–Fe_3O_4 powder was pressed into a plate with a diameter of 1 cm and a thickness of 60 μm. Then, σ of the sample was measured with a Corners probe tester.

RESULTS AND DISCUSSION

Preparation of the GNS–Fe_3O_4/PI Films with Oriented GNS–Fe_3O_4

The XRD pattern of GNS–Fe_3O_4 is shown in Figure 2(a). Figure 2(a,II) shows the standard characteristic peaks of Fe_3O_4 (JCPDS 19-0629). These characteristic peaks were observed in the XRD pattern of the GNS–Fe_3O_4 hybrid [Figure 2(a,I)] and indicated the presence of Fe_3O_4. The average particle size of Fe_3O_4 was 2.8 nm, as calculated by Scherrer's equation on the basis of the (331) crystalline peak shown in Figure 2(a,I). The TEM image of GNS–Fe_3O_4 [Figure 2(b)] shows that the surface of the GNSs was evenly decorated with Fe_3O_4 nanoparticles. The size of Fe_3O_4 was less than 5 nm and was in accordance with the results of XRD. The saturation magnetization of the prepared GNS–Fe_3O_4 was about 13 emu/g [Figure 2(c)]. All of the data described previously showed the successful formation of GNS–Fe_3O_4.[28]

In the scanning electron micrographs of H-GNS–Fe_3O_4/PI and P-GNS–Fe_3O_4/PI with 5 wt % GNS–Fe_3O_4 [Figure 3(a–d)], the flexible GNSs were parallel to each other and were considered to be a wrinkling trend of GNS–Fe_3O_4, although in N-GNS–Fe_3O_4/PI, the wrinkling of GNS–Fe_3O_4 appeared to be irregular [Figure 3(e,f)]. The orientation degrees of H-GNS–Fe_3O_4/PI and P-GNS–Fe_3O_4/PI were better than that of N-GNS–Fe_3O_4/PI, so the orientation of the GNS sheets in the films was controlled as expected.

Dielectric Properties of the GNS–Fe_3O_4/PI Films with the Frequency and GNS–Fe_3O_4 Content

The k and dielectric loss values of the composite films with frequency are shown in Figure 4. When the content of GNS–Fe_3O_4 was 1 wt %, the k [Figure 4(a)] and dielectric loss [Figure 4(b)] values of H-GNS–Fe_3O_4/PI, P-GNS–Fe_3O_4/PI, and N-GNS–Fe_3O_4/PI almost did not change with frequencies lower than 2×10^5 Hz. The k decrease and the dielectric loss increase at frequencies higher than 10^5 Hz were due to the dielectric relaxation.[31] When the content of GNS–Fe_3O_4 was 3–7 wt %, the k values [Figure 4(c,e,g)] of the GNS–Fe_3O_4/PI films still showed little frequency dependence in all of the measured frequency region; this was beneficial for their wide applications. Although the dielectric loss of these films [Figure 4(f,h)] was much higher at low frequencies and then decreased to level off, the higher dielectric loss at lower frequencies was mainly from the interfacial polarization, which could not follow the frequency switch at higher frequencies and decreased gradually. When the content of GNS–Fe_3O_4 was up to 10 wt %, not only the dielectric loss [Figure 4(m)] but also k [Figure 4(i)] of the film depended greatly on the frequency. The high k decreased dramatically with frequency compared to the films with lower GNS–Fe_3O_4. Under an electric field, the GNS interlayer was easily polarized and accumulated negative charges.[32] Under a higher content of GNS–Fe_3O_4, this kind of interface polarization became more dominant and gave target films with high k values. The changes in k and the dielectric loss with frequency showed that the dielectric loss relied more on the frequency than on k at low frequency.

To clearly determine the principle of k and dielectric loss with GNS–Fe_3O_4content, especially with the orientation of GNS–Fe_3O_4, the k and dielectric loss of the composites at 10^3 and 10^6 Hz are summarized in Figure 5. Figure 5(a,b) presents the

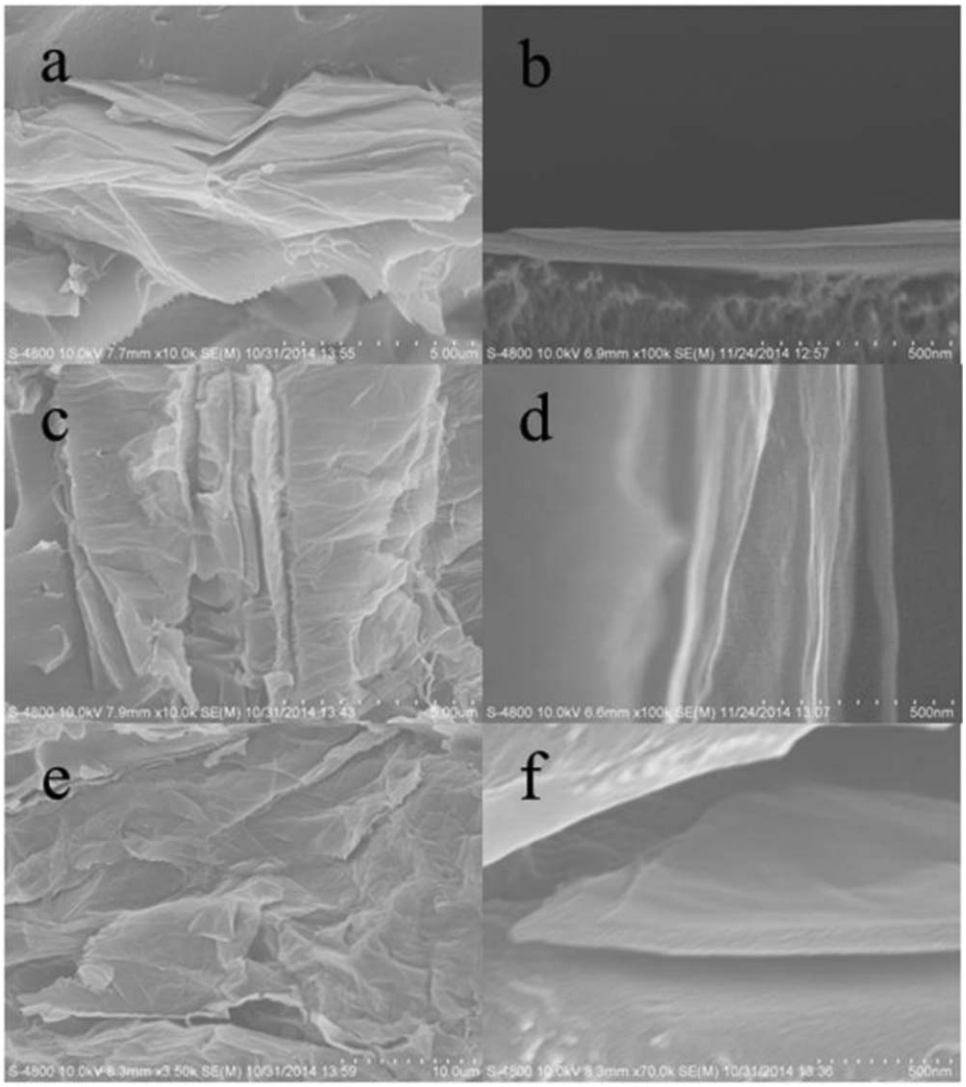

Figure 3. Fracture surface morphology of (a,b) H-GNS–Fe_3O_4/PI, (c,d) P-GNS–Fe_3O_4/PI, and (e,f) N-GNS–Fe_3O_4/PI with 5 wt % GNS–Fe_3O_4.

dielectric properties of the GNS–Fe_3O_4/PI films as a function of the GNS–Fe_3O_4 content at 10^3 Hz. The k showed a sudden, giant increase when the content of GNS–Fe_3O_4 in the composite was greater than 7 wt %. On the basis of percolation theory,[9,33] 7 wt % GNS–Fe_3O_4 was set as the percolation threshold. Beyond the percolation threshold, the GNS–Fe_3O_4 molecules could not effectively contact one another to form electrical paths. When the content of GNS–Fe_3O_4 was about 7 wt %, electrical paths were formed, but most of the GNS–Fe_3O_4 was still separated by a thin layer of polymer matrix.[34] This resulted in an obvious k increase to 1170. With a further increase in GNS–Fe_3O_4, σ of GNS–Fe_3O_4 caused the film to be a conductor. When the GNS–Fe_3O_4/PI composites were conductor/polymer composites. σ of GNS–Fe_3O_4 was 1.7×10^{-5} S/m, and PI was insulating polymer. The σ values of the films with GNS–Fe_3O_4 were studied (Figure 6). When the content of GNS–Fe_3O_4 was not more than 5 wt %, the σ values of the films changed little. When the content of GNS–Fe_3O_4 was further increased, a sudden increase in σ was observed; this was attributed to the connection of a large amount of GNS–Fe_3O_4 and the formation of conductive networks.[35] When the content of GNS–Fe_3O_4 reached 10%, σ was almost 4×10^{-7} S/m; this was caused by the formation of physical GNS–Fe_3O_4 electrical paths.[34] For an electronic conductor/polymer system, the dielectric loss mainly consisted of the conduction loss and polarization loss of space charges.[31] Generally, the former makes a greater contribution to the dielectric loss than the latter. When conductive paths have not yet been formed, the interface between the polymer and the GNS–Fe_3O_4 sheets hindered the charge transportation from one GNS–Fe_3O_4 sheet to another, so the influence of the conduction loss on the dielectric loss of the composites was low. When the content of GNS–Fe_3O_4 increased to 5–10 wt %, conductive paths were formed because of the large length–diameter ratio and flexible GNS–Fe_3O_4 sheets in some region. Under an alternating-current electric field, electrons must pass a long road to reach a stable state; this causes a more and more obvious conduction loss, and the dielectric loss increases gradually.

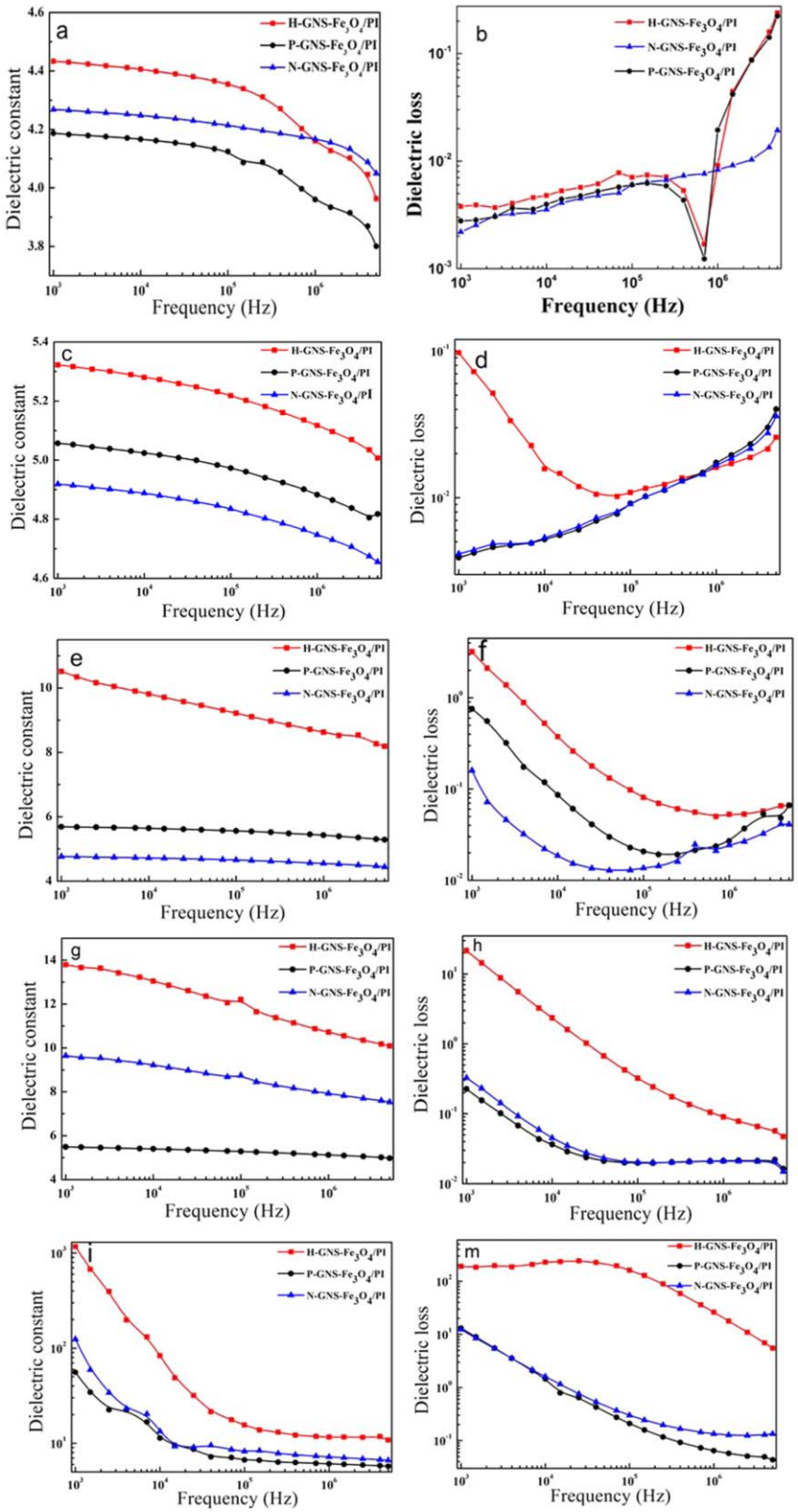

Figure 4. (a,c,e,g,i) *k* and (b,d,f,h,m) dielectric loss values of the GNS–Fe_3O_4/PI films with (a,b) 1, (c,d) 3, (e,f) 5, (g,h) 7, and (i,m) 10 wt % GNS–Fe_3O_4. [Color figure can be viewed in the online issue, which is available at wileyonlinelibrary.com.]

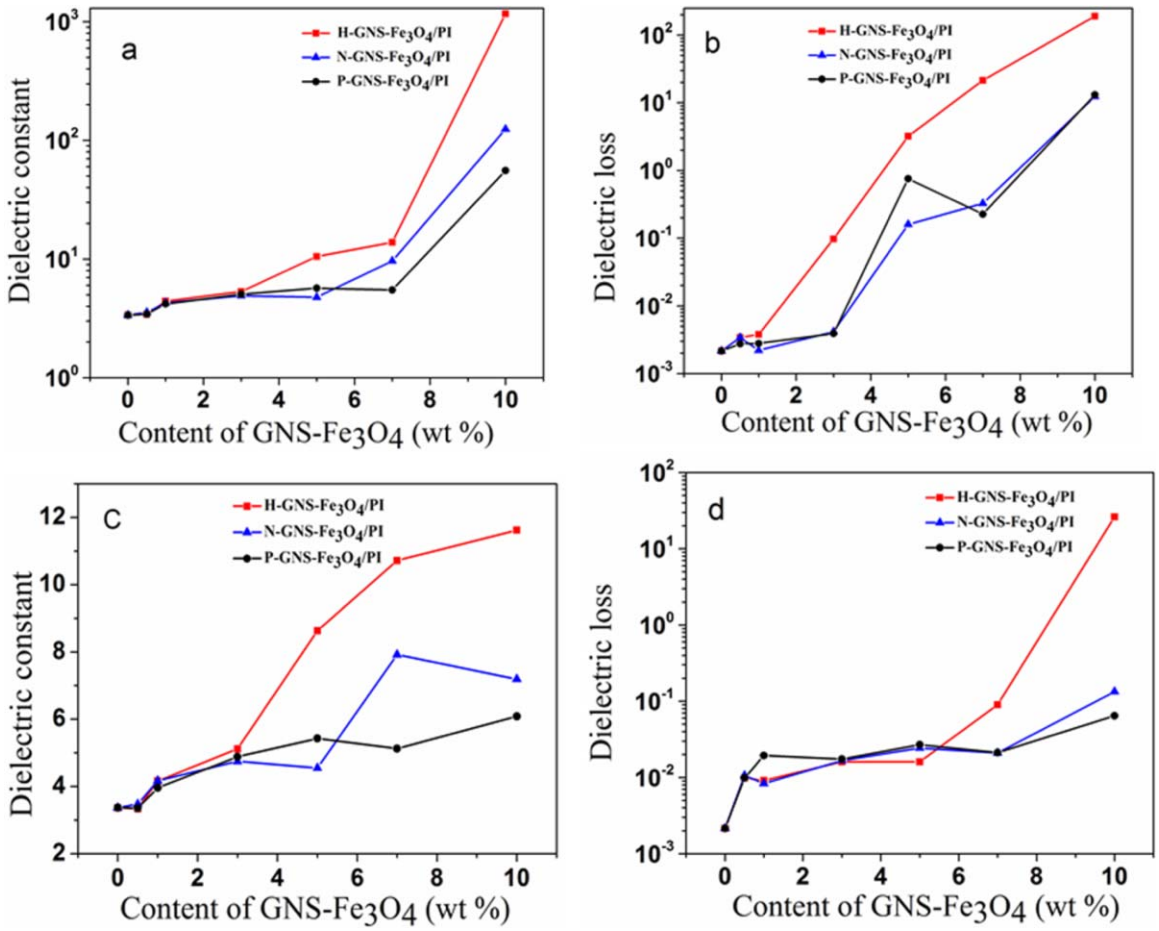

Figure 5. (a,c) k and (b,d) dielectric loss values of the GNS–Fe_3O_4/PI films as a function of the GNS–Fe_3O_4 content at (a,b) 10^3 and (c,d) 10^6 Hz. [Color figure can be viewed in the online issue, which is available at wileyonlinelibrary.com.]

The k and dielectric loss of GNS–Fe_3O_4/PI composite films at 10^6 Hz shown in Figure 5(c,d) were different from that at 10^3 Hz; the k enhancement of all of the films was not as high as that at 10^3 Hz. Also, the dielectric loss did not obviously rely on the GNS–Fe_3O_4 content. Only the H-GNS–Fe_3O_4/PI films showed a sudden, giant increase with the content of GNS–Fe_3O_4, which also showed a left shift. When the measurement frequency was 10^6 Hz, some nanometer capacitors were broken down and transferred to a conductive system. So. the work frequency of the nanometer capacitors decreased to a lower frequency, and the percolation threshold left-shifted. At 10^6 Hz, only the H-GNS–Fe_3O_4/PI films showed a percolation threshold; this was because of the regular arrangement of GNS–Fe_3O_4, which fabricated lots of effective capacitors. However, at a higher frequency, interfacial polarization was avoided, and this resulted in little dependence of k and the dielectric loss on the GNS–Fe_3O_4 content.

Influence of the Orientation on the Dielectric Properties of the GNS–Fe_3O_4/PI Films

At 10^3 Hz [Figure 5(a,b)], when the content of GNS–Fe_3O_4 was lower than 5 wt %, the orientation of GNS–Fe_3O_4 had little influence on the dielectric properties of the composite films. However, when the content of GNS–Fe_3O_4 increased further, the k values of the H-GNS–Fe_3O_4/PI films, especially those of the composites with higher contents of GNS–Fe_3O_4, were obviously higher than those of N-GNS–Fe_3O_4/PI and P-GNS–Fe_3O_4/

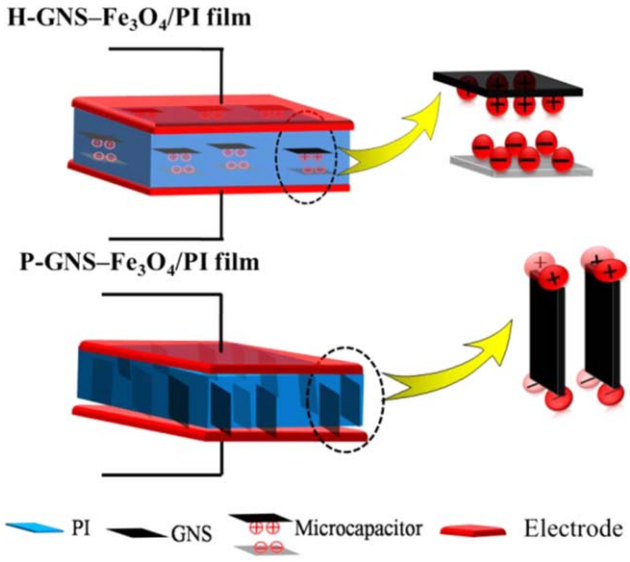

Figure 6. σ values of the GNS–Fe_3O_4/PI films. [Color figure can be viewed in the online issue, which is available at wileyonlinelibrary.com.]

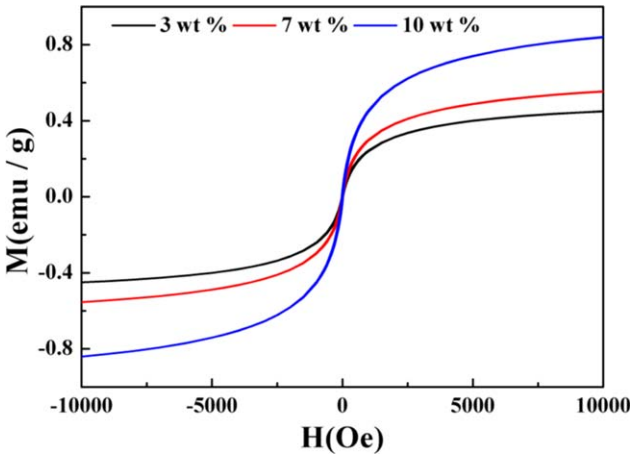

Figure 7. Polarization differences of H-GNS–Fe_3O_4/PI and P-GNS–Fe_3O_4/PI. "H" and "P" represent the film was oriented horizontal or perpendicular to the glass slide surface with an approximately 0.6-T magnetic field. [Color figure can be viewed in the online issue, which is available at wileyonlinelibrary.com.]

PI. The *k* values of the anisotropic films with the same amount of GNS–Fe_3O_4 were in the order H-GNS–Fe_3O_4/PI > N-GNS–Fe_3O_4/PI > P-GNS–Fe_3O_4/PI films. The *k* value of H-GNS–Fe_3O_4/PI with 10 wt % GNS–Fe_3O_4 was as high as 1170.3; this was about 355 times that of pure PI (3.3), 9.4 times that of N-GNS–Fe_3O_4/PI (124.4), and 21 times that of P-GNS–Fe_3O_4/PI (55.8). The highest *k* was higher than the reported one ($k = 123$) when the influence of the polymer matrix was ignored.[27] However, the dielectric loss of H-GNS–Fe_3O_4/PI was also obviously higher than those of N-GNS–Fe_3O_4/PI and P-GNS–Fe_3O_4/PI. The latter two kinds of films almost possessed the same dielectric losses. This interesting phenomenon originated from the different microstructures of the anisotropic GNS–Fe_3O_4/PI films. It was reported that when the content of GNS–Fe_3O_4 was 10.69 vol %, which was above the percolation threshold, the dielectric loss of GNS–Fe_3O_4/PS was 85.[27] These data were also relatively high because of the formation of many conductive paths. Although GNS is considered to be composed of conductive particles, it is different than metal. Maybe because GNS can more easily be dispersed in a polymer matrix as nanoparticles than metal particles, large interfaces between GNS and polymer forms which cause large dielectric losses.

As shown in Figure 7, in the H-GNS–Fe_3O_4/PIs, the GNS sheets were parallel to the film surface and stacked layer by layer in a sandwich form. The GNS sheets were isolated by polymer thin layers, and more nanocapacitors formed. Under an alternating-current electric field, all of the lateral surfaces of the GNSs could polarize to contain negative charges, although in the P-GNS–Fe_3O_4/PIs, a number of microcapacitors could still be formed, but the surface for the accumulation of charge could only be the terminal surface of GNS because GNS is perpendicular to the film surface. So, the accumulation surface for charges in the P-GNS–Fe_3O_4/PIs was much less than that in the H-GNS–Fe_3O_4/PIs. In H-GNS–Fe_3O_4/PI, more dipoles switched with the measurement of electric field; this resulted in a higher conduction loss. As the dielectric loss is mainly derived from polarization loss and conduction loss, it is preferred that perfect films with horizontal GNS–Fe_3O_4 are prepared, so the conduction loss can be mostly resisted. However, in the real sample, some conductive paths in certain regions could not be avoided. So, in some region of H-GNS–Fe_3O_4/PI, a zigzag path formed for electrons to pass into the stable polarization interface. This caused a higher conduction loss than in the other samples.

The *k* values of P-GNS–Fe_3O_4/PIs showed little difference from those of the N-GNS–Fe_3O_4/PIs with lower fillers and were slightly lower than those of the N-GNS–Fe_3O_4/PIs with more N-GNS–Fe_3O_4, but their dielectric losses were almost equal. In the orientation process, the magnetic field force and the gravitational force coexisted in the system. The magnetic force and gravitational force were all intended to run the sheets parallel to the film surface in the formation of the H-GNS–Fe_3O_4/PIs, although for the P-GNS–Fe_3O_4/PIs, the magnetic force made the sheets perpendicular to the film surface, and the gravitational force drove the sheets parallel to the film surface during solution flow and solvent evaporation.[29,36] So, in the P-GNS–Fe_3O_4/PIs, the parallel microcapacitors were not as good as those in the H-GNS–Fe_3O_4/PIs. The flawed film structure and small effective area for polarization contributed little to the polarization of the film, so the *k* values of the P-GNS-Fe_3O_4/PIs were slightly lower than those of the N-GNS–Fe_3O_4/PIs at 10^3 Hz.

At a higher frequency (10^6 Hz), the *k* values of H-GNS–Fe_3O_4/PIs were not as high as those at 10^3 Hz but were still obviously higher than those of the P-GNS–Fe_3O_4/PIs and N-GNS–Fe_3O_4/PIs as the more effective nanocapacitors were in the H-GNS–Fe_3O_4/PIs. More GNS–Fe_3O_4 sheets resulted in a lower arrangement difference between the P-GNS–Fe_3O_4/PIs and N-GNS–Fe_3O_4/PIs, so the *k* values of the N-GNS–Fe_3O_4/PIs were not much higher than those of the P-GNS–Fe_3O_4/PIs in contrast to those at 10^3 Hz. Meanwhile, the dielectric losses of the N-GNS–Fe_3O_4/PIs and P-GNS–Fe_3O_4/PIs were not greatly different.

Magnetic Properties of the GNS–Fe_3O_4/PI Films

Polymer composites with good magnetic, electrical, and dielectric performances have great potential in electromagnetic applications.[27] Figure 8 show the saturation magnetization of the

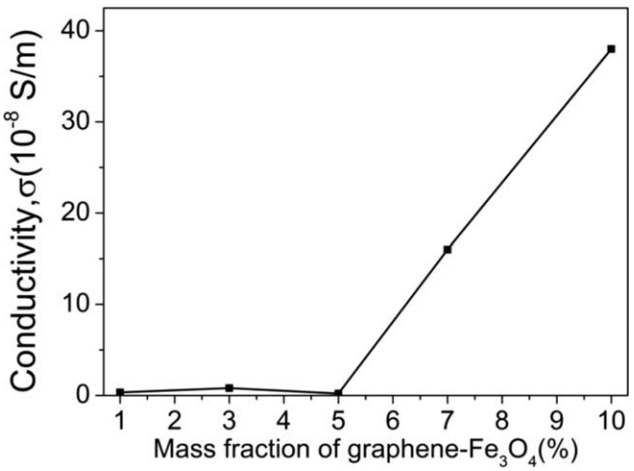

Figure 8. Magnetization hysteresis loops of the GNS–Fe_3O_4/PI composites at room temperature with (a) 3, (b) 7, and (c) 10 wt % GNS–Fe_3O_4.

GNS–Fe_3O_4/PI films with different contents of GNS–Fe_3O_4. The saturation magnetization of the films containing 7 and 10 wt % GNS–Fe_3O_4 were 0.43 and 0.84emu/g and could respond to a strong external magnetic field.

CONCLUSIONS

A series of GNS–Fe_3O_4/PI composite films with oriented GNS sheets were successfully prepared. The effects of the orientation of GNS–Fe_3O_4, the content of GNS–Fe_3O_4, and the frequency on the dielectric properties of the films were studied in detail. The dielectric property differences of the H-GNS–Fe_3O_4/PIs, N-GNS–Fe_3O_4/PIs, and P-GNS–Fe_3O_4/PIs were not obvious when the content of GNS–Fe_3O_4 was lower than 5 wt %. However, at the percolation threshold, the k values were in the order H-GNS–Fe_3O_4/PI > N-GNS–Fe_3O_4/PI > P-GNS–Fe_3O_4/PI in films with the same amount of filler. k of H-GNS–Fe_3O_4/PI with 10 wt % GNS sheets was as high as 1170.3 at 10^3 Hz and about 10 times that of P-GNS–Fe_3O_4/PI (124.4). The higher k of H-GNS–Fe_3O_4/PI was derived from the fabrication of more effective microcapcitors by GNS sheets, which were parallel to the film surface because of the orientation by the magnetic field; this means that microcapacitors perpendicular to the surface were useless to k enhancement. The switching of more charges on the lateral surface of GNS in the H-GNS–Fe_3O_4/PIs with electric field also caused a higher dielectric loss and the frequency dependence of k and the dielectric loss. These results are useful for the effective utilization of fillers for the preparation of functional materials.

ACKNOWLEDGMENTS

The work was financially supported by the Fundamental Research Funds for the Central Universities (contract grant number 2-9-2013-49) and National High Technology Research and Development Program (863 Program contract grant number 2012AA06A109).

REFERENCES

1. Arbatti, M.; Shan, X.; Cheng, Z. Y. *Adv. Mater.* **2007**, *19*, 1369.
2. Yu, Y.-Y.; Liu, C.-L.; Chen, Y.-C.; Chiu, Y.-C.; Chen, W.-C. *RSC Adv.* **2014**, *4*, 62132.
3. Chen, Y.; Xia, Y.; Sun, H.; Smith, G. M.; Yang, D.; Ma, D.; Carroll, D. L. *Adv. Funct. Mater.* **2014**, *24*, 1501.
4. Kim, Y. S.; Smith, O. L.; Kathaperumal, M.; Johnstone, L. R.; Pan, M. J.; Perry, J. W. *RSC Adv.* **2014**, *4*, 19668.
5. Zhang, Q.; Li, H.; Poh, M.; Xia, F.; Cheng, Z.-Y.; Xu, H.; Huang, C. *J Mater. Sci. Mater. Electron.* **2012**, *23*, 1504.
6. Chu, B.; Zhou, X.; Ren, K.; Neese, B.; Lin, M.; Wang, Q.; Bauer, F.; Zhang, Q. M. *Science* **2016**, *313*, 334.
7. Dang, Z. M.; Yuan, J. K.; Yao, S. H.; Liao, R. *J. Adv. Mater.* **2013**, *25*, 6334.
8. Huang, X.; Jiang, P. *Adv. Mater.* **2015**, *3*, 546.
9. Yu, L.; Zhang, Y.; Tong, W.; Shang, J.; Shen, B.; Lv, F.; Paul, K. *RSC Adv.* **2011**, *2*, 8793.
10. He, F.; Lau, S.; Chan, H. L.; Fan, J. *Adv. Mater.* **2009**, *21*, 710.
11. Gu, L.; Liang, G.; Shen, Y.; Gu, A.; Yuan, L. *Compos. B* **2014**, *58*, 66.
12. Panda, M.; Srinivas, V.; Thakur, A. *Appl. Phys. Lett.* **2008**, *92*, 132905.
13. Shen, Y.; Lin, Y.; Nan, C. W. *Adv. Funct. Mater.* **2007**, *17*, 2405.
14. Hayashida, K. *Composites* **2013**, *3*, 221.
15. Liu, H.; Shen, Y.; Song, Y.; Nan, C. W.; Lin, Y.; Yang, X. *Adv. Mater.* **2011**, *23*, 5104.
16. Chen, Q.; Du, P.; Jin, L.; Weng, W.; Han, G. *Appl. Phys. Lett.* **2007**, *91*, 022912.
17. Kaczmarek, H.; Podgórski, A. *Polym. Degrad. Stab.* **2007**, *92*, 939.
18. Wang, B.; Jiao, Y.; Gu, A.; Liang, G.; Yuan, L. *Compos. Sci. Technol.* **2014**, *91*, 8.
19. Guo, H.-L.; Wang, X.-F.; Qian, Q.-Y.; Wang, F.-B.; Xia, X.-H. *ACS Nano* **2009**, *3*, 2653.
20. Huang, T.; Xin, Y.; Li, T.; Nutt, S.; Su, C.; Chen, H.; Liu, P.; Lai, Z. *Am. Chem. Soc. Appl. Mater. Interfaces* **2013**, *5*, 4878.
21. Yang, K.; Huang, X.; Fang, L.; He, J.; Jiang, P. *Nanoscale* **2014**, *6*, 14740.
22. Yousefi, N.; Sun, X.; Lin, X.; Shen, X.; Jia, J.; Zhang, B.; Tang, B.; Chan, M.; Kim, J. K. *Adv. Mater.* **2014**, *26*, 480.
23. Zheng, G.; Wu, J.; Wang, W.; Pan, C. *Carbon* **2004**, *42*, 2839.
24. Mack, J. J.; Viculis, L. M.; Ali, A.; Luoh, R.; Yang, G.; Hahn, H. T.; Ko, F. K.; Kaner, R. B. *Adv. Mater.* **2005**, *17*, 77.
25. Tong, W.; Zhang, Y.; Yu, L.; Luan, X.; An, Q.; Zhang, Q.; Lv, F.; Chu, P. K.; Shen, B.; Zhang, Z. *J. Phys. Chem. C.* **2014**, *118*, 10567.
26. Tian, M.; Wei, Z.; Zan, X.; Zhang, L.; Zhang, J.; Ma, Q.; Ning, N.; Nishi, T. *Compos. Sci. Technol.* **2014**, *99*, 37.
27. Kovtyukhova, N. I.; Ollivier, P. J.; Martin, B. R.; Mallouk, T. E.; Chizhik, S. A.; Buzaneva, E. V.; Gorchinskiy, A. D. *Chem. Mater.* **1999**, *11*, 771.
28. Park, S.; An, J.; Piner, R. D.; Jung, I.; Yang, D.; Velamakanni, A.; Nguyen, S. T.; Ruoff, R. S. *Mater. Chem.* **2008**, *20*, 6592.
29. Lv, F.; Xu, L.; Xu, Z.; Fu, L.; Zhang, Y. *J. Appl. Polym.* **2015**, DOI: 10.1002/app.41224.
30. Shang, J.; Zhang, Y.; Yu, L.; Shen, B.; Lv, F.; Chu, P. K. *Mater. Chem. Phys.* **2012**, *134*, 867.
31. Kim, J. Y.; Lee, J.; Lee, W. H.; Kholmanov, I. N.; Suk, J. W.; Kim, T.; Hao, Y.; Chou, H.; Akinwande, D.; Ruoff, R. S. *ACS Nano* **2014**, *8*, 269.
32. Yang, K.; Huang, X.; Zhu, M.; Xie, L.; Tanaka, T.; Jiang, P. *Am. Chem. Soc. Appl. Mater. Interfaces* **2014**, *6*, 1812.
33. Shen, Y.; Lin, Y.; Li, M.; Nan, C. W. *Adv. Mater.* **2007**, *19*, 1418.
34. He, F.; Lam, K.; Ma, D.; Fan, J.; Chan, L. H.; Zhang, L. *Carbon* **2013**, *58*, 175.
35. Xu, W.; Ding, Y.; Jiang, S.; Zhu, J.; Ye, W.; Shen, Y.; Hou, H. *Eur. Polym. J.* **2014**, *59*, 129.
36. Ansari, S.; Kelarakis, A.; Estevez, L.; Giannelis, E. P. *Small* **2010**, *6*, 205.